Compressed sensing in synthetic aperture photoacoustic tomography based on a linear-array ultrasound transducer

Xiangwei Lin (蔺祥伟)[1], Naizhang Feng (冯乃章)[1], Yawei Qu (屈亚威)[2], Deying Chen (陈德应)[3], Yi Shen (沈 毅)[1], and Mingjian Sun (孙明健)[1,*]

[1]*Department of Control Science and Engineering, Harbin Institute of Technology, Harbin 150001, China*
[2]*Department of Gastroenterology, General Hospital of Chinese People's Armed Police Forces, Beijing 100039, China*
[3]*Institute of Opto-electronics, Harbin Institute of Technology, Harbin 150080, China*
**Corresponding author: sunmingjian@hit.edu.cn*

Received May 15, 2017; accepted July 14, 2017; posted online August 11, 2017

Photoacoustic tomography (PAT) has the unique capability of visualizing optical absorption inside several centimeters-deep biological tissue with a high spatial resolution. However, single linear-array transducer-based PAT suffers from the limited-view challenge, and thus the synthetic aperture configuration is designed that still requires multichannel data acquisition hardware. Herein, a feasible synthetic aperture PAT based on compressed sensing reconstruction is proposed. Both the simulation and experimental results tested the theoretical model and validated that this approach can improve the image resolution and address the limited-view problem while preserving the target information with a fewer number of measurements.

OCIS codes: 110.5120, 100.3020, 170.5120, 170.0110.
doi: 10.3788/COL201715.101102.

Photoacoustic (PA) imaging is a noninvasive imaging modality based on the thermoelastic expansion effect in biological tissues. This imaging tool could provide anatomical, functional, metabolic, molecular, and genetic contrasts from organelles to organs[1–4]. Due to the weaker scattering of acoustic propagation compared with light diffusion in biological tissue, photoacoustic tomography (PAT) has the unique capability of visualizing optical absorption in deep tissues up to several centimeters while still maintaining high acoustic spatial resolution[5–7]. The linear-array ultrasound transducer-based PAT is most widely used because it has accelerated imaging speed, bedside availability, and shared hardware platform with the B-mode ultrasound in nature[1,3].

One of the main concerns in the linear-array transducer based PAT is that this modality suffers from the limited-view challenge[8–11], especially in tracing the vessel structure in biological tissue[12]. A full ring or concave array transducer[13,14] could acquire a full-view dataset, but they are expensively custom made and cannot be modified once fabricated. Wang's group chose an acoustic reflector to increase the detection angle, either one reflector placed at 45°[15] or two reflectors located at 120° to triple the detection view[16]. Cox *et al.* also used acoustic reflectors[17] and a reverberant cavity[18] to enhance the view of the planar array. Kruger *et al.* focused on the relative rotation between the transducer and sample to enlarge the detection coverage, rotating either the target[19] or the transducer[20]. Nonetheless, these methods are favorable to acquiring complete data but cannot always be realized on clinic, which are limited by the data acquisition (DAQ) channel number, target structure, and the acoustic coupling medium such as the cervical vessel cannot be accessed from all directions.

The limited-view problem could be compensated if the synthetic aperture detection configuration is established to encircle the target. The original incomplete detection geometry of the single-array transducer would be effectively extended based on the spatial compounding method[21,22]. However, the synthetic aperture setup would inevitably increase the burden of DAQ hardware. As the number of transducer elements increases, the operation and reconstruction in the ultrasound receiving system become more challenging and costly[23]. Compressed sensing (CS) could recover compressible signals from under-sampled measurements, and thus it is suitable for PA image reconstruction from insufficient measurements[24–27]. Therefore, the CS method could accelerate the data acquisition speed and reduce the cost of DAQ hardware in the synthetic aperture PAT.

In this Letter, a feasible synthetic aperture PAT configuration based on the CS reconstruction algorithm is proposed. This approach combined the ultrasound spatial compounding method to extend the effective aperture size and the CS technique to reduce the measurement dataset. The theoretical model of the limited-view issue in the linear-array transducer based PAT was first introduced, then the corresponding simulation and phantom studies were conducted to verify the synthetic aperture setup and the proposed CS reconstruction method.

The generation of acoustic waves is resulted from the PA effect in the biological tissue. Through the instant excitation of a short-pulsed laser, a certain proportion of the absorbed energy would be converted into heat, generating

a wideband acoustic signal due to the transient thermoelastic expansion. The mathematical model for the forward problem of PAT in an acoustically homogeneous tissue in the case of thermal confinement is

$$p_d(r_d, t) = \frac{1}{4\pi c}\frac{\partial}{\partial t}\int \mathrm{d}A \frac{p_0(r)}{|r_d - r|}\bigg|_{ct=|r_d-r|}. \quad (1)$$

The pressure p_d in the detection surface at a spatial point r_d and time t is proportional to the time derivative of the integral of the absorbed laser energy over a spherical surface (a circle in the 2D case) centered at r_d and with radius ct. The forward generation and closed detection trajectory of the PA signal are shown in Fig. 1(a). The PA signals are then detected and reconstructed to represent the optical absorption distribution. The initial PA energy distribution recovered by the universal back projection (BP) method[28] is

$$p_0(r) = \frac{1}{4\pi c^2}\int \mathrm{d}S \frac{1}{t}\left[\frac{p_d(r_d, t)}{t} - \frac{\partial p_d(r_d, t)}{\partial t}\right]\bigg|_{ct=|r_d-r|}. \quad (2)$$

Both the PA signal detection and PA image reconstruction assume that the detection trajectory should be an enclosed surface with infinitely small point detectors. This is contradictory to the practical application, where the spatial sampling interval always exists in a single element or an array transducer. An infinitely wide array is demanded to entirely cover the target if linear array is considered. However, in practice, the aperture size of the probe and the penetrated depth of the PA wave are finite and restricted. As a result, the synthetic aperture configuration composed by a single linear-array transducer was proposed and the concept model to detect the artificial blood vessels is illustrated in Fig. 1(b) intuitively.

It can be observed that the generated PA signals will only be detected at two opposite orientations of the omnidirectional propagation. So the target boundary located at the real red part can be detected by the transducer, while the green dashed part presents the missing information of the target. The finite aperture size could not collect the entire acoustic signal, leading to the loss of structure information, limited-view artifacts, and image resolution degradation. Here, the tilted angle of the extended aperture is assigned as 60°, considering the target structure, imaging depth, and geometrical symmetry of the field of view (FOV). Thus the three linear-array transducers would form the semicircle cross-sectional geometry to approximate enclosed detection surface and then the multiview data will be collected. However, a multi-element ultrasound transducer and the associated multichannel DAQ electronics will be required to receive the PA signals. Therefore, to reduce the hardware cost and improve data acquisition speed, the CS technique has been applied here to reconstruct an image with fewer measurements. The selected receiving channels in CS reconstruction are shown as the dark blue element in Fig. 1(b).

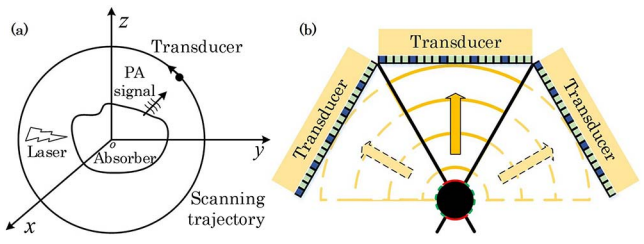

Fig. 1. Theoretical model of the synthetic aperture PAT. (a) Ideal PA signal generation and detection. (b) Synthetic aperture configuration with 1/4 DAQ channels.

CS is suitable for sparse reconstruction from incoherent measurements. The images in PAT are speckle-free and sensitive to the boundaries of the absorbers[29,30]. So the image θ to be recovered is sparse in nature and could be transformed through the sparse matrix Ψ to get its sparse representation x. The forward problem of PAT can be seen as projecting the transformed object x through the measurement matrix Φ, and the received data y is the corresponding matrix multiplication result. Based on the BP principle, the measurement matrix in the time domain can be formed as

$$\Phi(m, t)_{(i,j)} = \frac{1}{2\pi c}\delta\left(t - \frac{|r_{i,j} - r_m|}{c}\right), \quad m = 1, 2, ..., p;\ t = s\Delta t,\ s = 1, 2, ...q_s, \quad (3)$$

where $r_{i,j}$ represent the Cartesian coordinates of the image pixels, r_m is the position of the transducer, c is the speed of sound, p is the number of receiving channels, Δt is the sampling interval, and q_s is the number of sampling points. As a sequence, Eqs. (1) and (2) can be discretized to numerically model the forward and inverse problem as

$$y = \Phi\theta, \quad x = \Psi\theta, \quad (4)$$

$$\arg\min F = \|\Phi\Psi^{-1}x - y\|_2^2 + \alpha\|x\|_1, \quad (5)$$

where $\|\cdot\|_2$ is the l_2 norm and $\|\cdot\|_1$ is the l_1 norm. The first part keeps the fidelity between the recovered data and the raw data, and the second part maintains the sparsity of the signal. A nonlinear conjugate gradient descent method was adopted to solve the optimized solution, as detailed in Ref. [25]. The computation was running on a laptop with a dual-core 2.30 GHz, 4 GB memory and the calculation usually took less than 6 minutes with MATLAB 2012a.

In order to approximate the enclosed detection trajectory by only one single-aperture linear-array transducer, the conceptual model of the synthetic aperture PAT was proposed and verified numerically. The K-wave toolbox was chosen for simulation of the forward PA wave propagation and detection. The corresponding PA images were reconstructed by the CS method, with the traditional universal BP as a standard for comparison. The conceptual model of synthetic aperture configuration for imaging

the point targets and the artificial blood vessels are illustrated in Figs. 2(a) and 2(b), respectively. Three point targets were placed at the center FOV to test the resolution and a 2D model of disk target was used as the vessel sample in the limited view problem. The single center aperture smeared into a pale yellow background was chosen as the comparison with the synthetic aperture.

The synthetic aperture configuration consists of three linear-array transducers to acquire the PA signals simultaneously. It has 96 elements in total, each single linear array containing 32 directional elements. The pitch in each transducer is 0.304 mm and the center frequency is 7.5 MHz. The pitch size and the element width were maintained the same with the parameter of the transducer used in the following experiment. The properties of the acoustic source in the medium were defined as a spatially smoothed initial pressure distribution, assuming the radiation light was illuminated uniformly at the target.

In the first simulation, a series of point targets was placed to quantitatively measure the resolution determined by the different reconstruction methods. Distribution of the point sources in the synthetic aperture setup allowed for analysis of the beam profile along the lateral axis of the array. The recovered PA images are separately shown in Fig. 3. The PA images shown in Figs. 3(a) and 3(b) are reconstructed by the BP method with a center aperture and a synthetic aperture separately. Figures 3(c) and 3(d) are images recovered by CS with full DAQ channels and one quarter DAQ channels, respectively.

It could be obviously seen that the image resolution from the synthetic aperture configuration was enhanced. Compare Fig. 3(d) with Fig. 3(a), the spatial resolution in the CS reconstructed image with only 1/4 of the total number of channels has ~128% improvement. Based on the spatially compounding principle, it is possible to achieve a higher resolution at deep regions in the multi-view setup. To ensure these point targets in the PA images would be clearly visualized, the reduced channel number in CS was determined by the lateral profile in Fig. 3(e). If contrast to noise ratio in the image with the one quarter channel (~20 dB) continue decreases, these point targets could not be distinguished from the background. This number was also applied in the following simulation and phantom study.

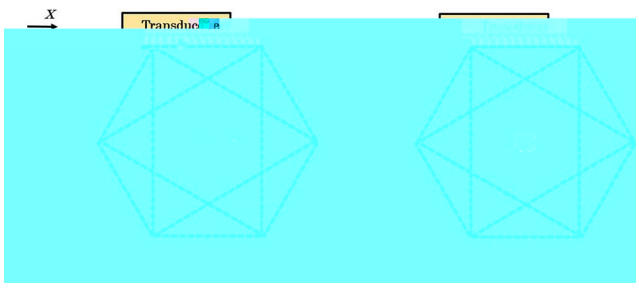

Fig. 2. Conceptual model of synthetic aperture PAT. (a) Image resolution simulation. (b) Limited-view simulation.

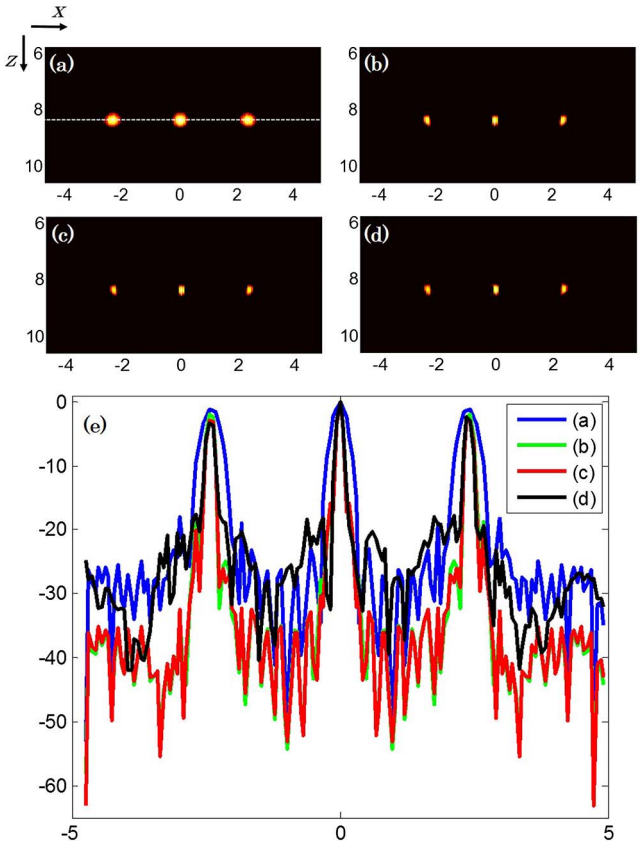

Fig. 3. (Color online) Enhanced resolution simulation results. The PA images reconstructed by (a) BP with center aperture, (b) BP with synthetic aperture, (c) CS with synthetic aperture, and (d) CS with 1/4 synthetic aperture. (e) The profile along the center line on (a)–(d).

Figures 4(a)–4(d) are the PA images of a numerical disk, which corresponds the conceptual model of artificial blood vessel with the synthetic aperture configuration in Fig. 2(b). Figures 4(a) and 4(b) demonstrate the results from the BP method, with 32 and 96 channels, respectively. From these two reference images, the PA image recovered from the single aperture PAT loses the target structure information due to the limited view deficiency, which matches our previous theoretical analysis.

Compare Fig. 4(a) with the others, the structure information is severely lost, while the vessel structure in the others can be clearly visualized with high image contrast. This happens because the effective physical size in the synthetic aperture is extended to approximate the closed detection surface. The target structure of the reconstructed images tends to be complete only if the extended angle is designed based on the geometric symmetry of the enclosed detection space. Compared with Figs. 4(b) and 4(c), the CS recovered image [i.e. Fig. 4(d)] with less DAQ receiving channels shows the similar image quality, considering the target position, geometrical structure and overall shape of the target, especially at the target boundary. These outcomes indicated this method can really improve the image qualities and compensate the lost structure, even though with one fourth of original measurements.

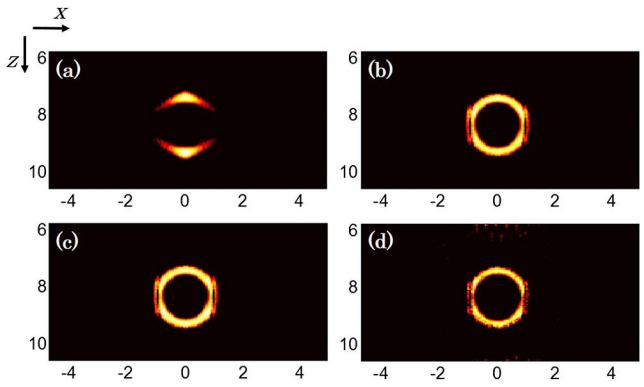

Fig. 4. Limited-view reconstruction results. (a) BP with center aperture, (b) BP with synthetic aperture, (c) CS with synthetic aperture, and (d) CS with 1/4 synthetic aperture.

Phantom studies were conducted to validate the feasibility of proposed method subsequently. To geometrically match the configuration in the simulation, the corresponding synthetic aperture setup was formed by rotating a single linear-array transducer, as shown in Fig. 5. An Nd:YAG laser (Vibrant 355 II HE, Opotek, Carlsbad, USA) emits a 5 ns width pulse with 10 Hz pulse repetition rate. The output light was delivered through the fiber bundle to ensure the uniform light illumination to the target. These bundles were integrated into the house-constructed transducer holder. The external trigger from the laser system was sent to synthesize the receive-only mode on the ultrasound array platform (Prodigy, S-Sharp, Taipei, China). A linear-array transducer with 7.5 MHz center frequency and 128 elements was rotated by a precise digital rotation platform (LSDH-100WS, Zolix, China) to acquire PA data.

The advantage of this single linear-array ultrasound transducer-based synthetic aperture PAT system is that the detection FOV can be easily adjusted. On the other hand, only one linear-array transducer was chosen to save the hardware resources. The system provides a potential solution for multiview imaging the larger and deeper region of interest in biological tissue, such as peripheral vessels, carotid artery. All the PA images were captured with a 780 nm wavelength and the maximum output laser fluence was limited to 15 mJ/cm^2. A small, point-like PA source (human hair with a diameter of 60 m) located in the center of the FOV was used to calibrate the coordination of the transducer elements first. This target could calibrate the synthetic aperture system and test the corresponding imaging resolution.

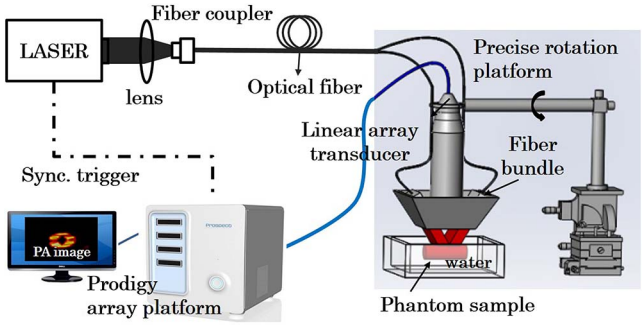

Fig. 5. PA experimental setup using a rotate-translate stage to form the synthetic aperture.

The relative position between the rotated linear-array transducer and reconstruction FOV should be determined first, especially the rotation center and rotation radius. These two parameters were determined by the aperture size of the transducer and controlled by the precise rotation platform. The rotation radius was 32.98 mm and the rotation center was located at the overlapped point of the three different views. The different rotating orientations were −60°, 0°, 60° separately, which were well matched with both the theoretical and numerical model, except the number of DAQ channels.

Figures 6(a) and 6(b) are the reconstructed PA images from BP method with center aperture and synthetic aperture, respectively. The CS reconstructed images are shown in Figs. 6(c) and 6(d). The element numbers in each case are all the elements (128×3) and one quarter elements ($1/4 \times 128 \times 3$). The element coordination in the synthetic aperture was ultimately obtained through this calibration process. In addition, better image resolution and side lobe reduction in Fig. 6(d) verifies the CS verifies the CS method could achieve an acceptable image quality with less DAQ measurements.

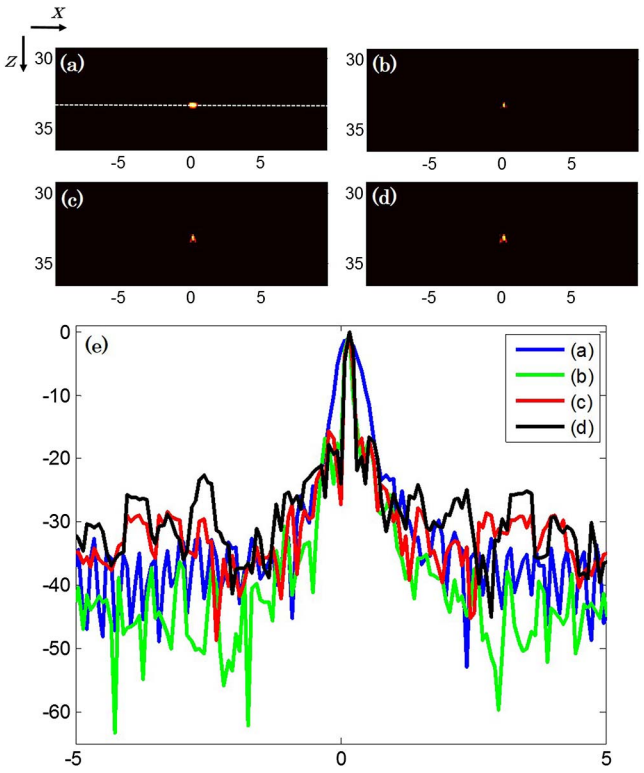

Fig. 6. (Color online) Enhanced resolution experiment results. (a) BP with a center aperture, (b) BP with a synthetic aperture, (c) CS with a synthetic aperture, and (d) CS with 1/4 synthetic aperture. (e) The profile along the center line on (a)–(d).

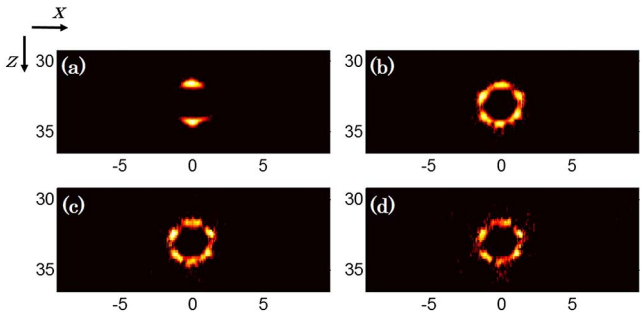

Fig. 7. Limited-view reconstruction results. (a) BP with center aperture, (b) BP with synthetic aperture, (c) CS with synthetic aperture, and (d) CS with 1/4 synthetic aperture.

After the calibration of this synthetic aperture system, a phantom experiment was performed. The aim is to test the feasibility of the synthetic aperture and CS method in tracing the vessel phantom. A polyethylene tube (inner diameter: 3.0 mm) filled with ICG (Indocyanine Green) was designed as the imaging target. This tube was embedded in the agar phantom at about 32.00 mm depth from the surface of the transducer. The light was distributed uniformly anda linear-array transducer was set as the predefined synthetic aperture to collect the PA data. The PA image in Fig. 7(a) shows the center aperture recovered result. Figures 7(b)–7(d) show more structure than the single aperture case. Thus, the synthetic aperture can really compensate the limited-view induced structure loss while maintaining the meaningful feature in the target. These results indicate that the synthetic aperture has the potential to overcome the limited-view challenge and it can provide approximate full-view imaging quality. Furthermore, Fig. 7(d) is the image reconstructed by CS reconstruction with only 1/4 of the total number of receiving channels. By aid of CS method, the DAQ channels could be reduced to a certain extent while remaining the approximated full-view imaging quality.

In conclusion, a synthetic aperture PAT configuration based on the CS reconstruction algorithm is proposed to improve the image resolution and address the limited view problem with fewer number of measurements. The detection coverage is enlarged due to the synthetic aperture and data acquisition channels are reduced due to the CS method. The theoretical analysis, simulation and phantom studies demonstrate that the PA image can be faster reconstructed with fewer channel data to achieve the nearly full-view image quality. In the current study, these off-line data processing methods just focus on recovering the satisfactory PA image quality with reduced measurements. In the future study, real time clinical feasibility for peripheral vessels and human breast imaging will be further investigated.

This work was partially supported by the National Natural Science Foundation of China (Nos. 61371045 and 11574064), the Shenzhen Science & Technology Program, China (No. JCYJ20160429115309834), and the Science and Technology Development Plan Project of Shandong Province, China (Nos. 2015GGX103016 and 2016GGX103032).

References

1. L. V. Wang and J. Yao, Nat. Methods **13**, 627 (2016).
2. A. A. Oraevsky, S. L. Jacques, R. O. Esenaliev, and F. K. Tittel, Proc. SPIE **2134**, 122 (1994).
3. C. Lutzweiler and D. Razansky, Sensors **13**, 7345 (2013).
4. B. Cox, J. G. Laufer, S. R. Arridge, and P. C. Beard, J. Biomed. Opt. **17**, 061202 (2012).
5. L. V. Wang and S. Hu, Science **335**, 1458 (2012).
6. J. Xia and L. V. Wang, IEEE Trans. Biomed. Eng. **61**, 1380 (2014).
7. L. V. Wang, Nat. Photonics **3**, 503 (2009).
8. Y. Xu, L. V. Wang, G. Ambartsoumian, and P. Kuchment, Med. Phys. **31**, 724 (2004).
9. M. Xu and L. V. Wang, Phys. Rev. E **67**, 056605 (2003).
10. M. Ye, M. Cao, J. Yuan, X. Liu, and X. Wang, Chin. Opt. Lett. **14**, 081701 (2016).
11. Y. Wang, J. Yuan, S. Du, X. Liu, and X. Wang, Chin. Opt. Lett. **13**, 061001 (2015).
12. M. P. Fronheiser, S. A. Ermilov, H. P. Brecht, A. Conjusteau, R. Su, K. Mehta, and A. A. Oraevsky, J. Biomed. Opt. **15**, 021305 (2010).
13. J. Xia, C. Huang, K. Maslov, M. A. Anastasio, and L. V. Wang, Opt. Lett. **38**, 3140 (2013).
14. E. Merčep, G. Jeng, S. Morscher, P. C. Li, and D. Razansky, IEEE Trans. Ultrason. Ferroelectron. Freq. Control **62**, 1651 (2015).
15. B. Huang, J. Xia, K. Maslov, and L. V. Wang, J. Biomed. Opt. **18**, 655 (2013).
16. G. Li, J. Xia, K. Wang, K. Maslov, M. A. Anastasio, and L. V. Wang, QIMS **5**, 57 (2014).
17. R. Ellwood, E. Zhang, P. Beard, and B. Cox, J. Biomed. Opt. **19**, 126012 (2014).
18. B. T. Cox, S. R. Arridge, and P. C. Beard, Inverse Probl. Eng. **23**, S95 (2007).
19. R. A. Kruger, W. I. Kiser, Jr., D. R. Reinecke, and G. A. Kruger, Med. Phys. **30**, 856 (2003).
20. B. Yin, D. Xing, Y. Wang, Y. Zeng, Y. Tan, and Q. Chen, Phys. Med. Biol. **49**, 1339 (2004).
21. G. R. Bashford and J. L. Morse, IEEE Trans. Med. Imag. **25**, 732 (2006).
22. H. K. Zhang, E. Ergun, G. E. Trahey, and E. M. Boctor, Proc. SPIE, **9419**, 94190L (2015).
23. M. K. Yapici, C. Kim, C. C. Chang, M. Jeon, Z. Guo, X. Cai, J. Zou, and L. V. Wang, J. Biomed. Opt. **17**, 116019 (2012).
24. C. L. Z. Guo, L. Song, and L. V. Wang, J. Biomed. Opt. **15**, 021311 (2010).
25. J. Meng, L. V. Wang, L. Ying, D. Liang, and L. Song, Opt. Express **20**, 16510 (2012).
26. D. L. Donoho, IEEE Trans. Inf. Theory **52**, 1289 (2006).
27. T. Liu, M. Sun, N. Feng, M. Wang, D. Chen, and Y. Shen, Chin. Opt. Lett. **14**, 091701 (2016).
28. M. Xu and L. V. Wang, Phys. Rev. E. Stat. Nonlin. Soft Matter Phys. **71**, 016706 (2005).
29. M. Haltmeier, T. Berer, S. Moon, and P. Burgholzer, J. Opt. **18**, 114004 (2016).
30. L. Ding, X. L. Deán-Ben, and D. Razansky, IEEE Trans. Med. Imag. **35**, 1883 (2016).